Study of structural and optical properties of $Ni_xCo_{1-x}Dy_yFe_{2-y}O_4$ nanomaterial synthesized by sol-gel autocumbustion method

Mahendra D. Waghmare[1,*,†], Sopan M. Rathod[2], Y. B. Khollam[3]

[1]Department of Physics, Modern College of Arts, Science and Commerce, Ganeshkhind. Pune 411007, Maharashtra, India.

[2]Department of Physics, Abasaheb Garware College, Erandwane, Pune 411004, Maharashtra, India.

[3]Department of Physics, Baburaoji Gholap College, Sangvi, Pune 411 027, Maharashtra, India.

Abstract

The present work reports the synthesis of ferrite powders having compositions: $Ni_xCo_{1-x}Dy_yFe_{2-y}O_4$, y = 0.025, x = 0, 0.1, 0.2, 0.3 and 0.4 by using nitrates of nickel, cobalt, dysprosium and, iron as starting materials. The preparation of ferrite powders was carried out into two steps. In first step the auto combustion of a gel obtained from stoichiometric mixture of starting materials with citric acid as burning agent was carried out. This was followed by the annealing of auto-combusted precursor at elevated temperature of 560 ^oC. The resultant as-annealed powders were characterized by the using different physical techniques: TGA/DTA, X-ray diffraction (XRD), UV-Visible spectroscopy, and FTIR spectroscopy. The temperature of ferrite was confirmed by using thermal analysis: TGA/DTA studies. The structural studies by using XRD revealed the formation of pure ferrite powders with cubic spinel symmetry. The values of the band gap by using UV-Visible spectroscopy were found to be in range of 1.638 to 1.673 eV. The FTIR spectra supported the XRD results.

Keywords: Ni-Co ferrite*;* Auto-combustion, UV-Visible, FTIR, TGA/DTA.

1. Introduction

The magnetic materials: ferrites have number of applications in field of sensors like magnetic magneto-electric and magneto-mechanical sensors. The cobalt and nickel based ferrites are having novel magnetostrictive properties. Hence, they are useful for the magneto-electric and magneto-mechanical sensors [1 - 6]. Further, photo-catalysis, high frequency devices, microwave devices, magnetically guided drug delivery are some of important applications of the spinel ferrites [7- 9]. The spinel ferrite can be made available for different applications by changing their properties with the help of doping these materials by rare-earth metals and different transition metals. The various applications of the ferrite depend on morphological features like size, shape and morphology of materials. Further, these morphological structural characteristics of ferrites are very sensitive to the method of the preparation, processing parameters, annealing

-sintering thermal profile, substitution different cations etc. [10 - 11]. The cation distribution at tetrahedral and octahedral sites of spinel structure depends upon the parameters used for processing of ferrites [11 - 12]. The cation distribution plays an important role in deciding the magnetic and electric properties like coercivity, saturation magnetization and electrical resistivity of the ferrites [13-14]. These magnetic and electric properties of ferrites are very useful for various applications like magnetic fluids, recording media, sensors and biomedical drug delivery [15-16]. The doping the spinel ferrites with rare earth ions modifies and improves the structural and magnetic properties of ferrites [17-18]. The ferrites doped with rare earth ions have number of applications in catalysis, magnetic storage and microwave devices [19-20]. The structural and magnetic properties of dysprosium doped ferrites are reported in literature [21-22]. However, the synthesis and measurement of properties of dysprosium doped ferrites are rarely studied in literature.

The different methods: co-precipitation, thermal decomposition, hydrothermal, sonochemical, sol–gel etc. are reported in literature for the synthesis of pure and doped ferrites [23 - 27]. These methods require number of processing steps and stringent control on various processing parameter. These methods are also end up with the annealing of as-prepared precursor at elevated temperature. However, the auto-combustion of co-precipitated precursor followed by annealing at elevated temperature is rather very simple and time saving method leading the final active material having phase purity and better stoichiometric control. In view of this, in present work, simple method comprising the auto-combustion of co-precipitated gel precursor followed annealing at elevated temperature is employed for the synthesis of dysprosium doped nickel-cobalt nano-crystalline ferrite. The results obtained pertaining to synthesis and characterizations of dysprosium doped nickel-cobalt nano-crystalline ferrite are presented in this communication.

2. Experimental

2.1. Materials

The ferric nitrate [$Fe(NO_3)_3$. $9H_2O$], Nickel nitrate [$Ni(NO_3)_2.6H_2O$], Cobalt Nitrate [$Co(NO_3)_2 \cdot 6H_2O$] and Dysprosium (III) nitrate hydrate [$Dy(NO_3)_3.xH_2O$] all from Loba Chemie, Pune and 99 % pure GR grade chemicals are used as the starting materials in present research work as received without further any purification.

2.2. Synthesis of ferrite powder

In the present work, the five different ferrite powders with compositions, $Ni_xCo_{1-x}Dy_yFe_{2-y}O_4$ where y = 0.025, and x = 0, 0.1, 0.2, 0.3, 0.4 were prepared by using the auto-combustion method. For the preparation of $Ni_xCo_{1-x}Dy_yFe_{2-y}O_4$ with x = 0.0 and y = 0.025, the stoichiometric amount molar solutions of $Fe(NO_3)_3.9H_2O$, $Ni(NO_3)_2.6H_2O$, $Co(NO_3)_2 \cdot 6H_2O$ and $Dy(NO_3)_3.xH_2O$ were prepared in double distilled water. Then all solutions were mixed together in equal amounts to obtain the resultant solution. To this final solution the citric acid was added as burning agent. The resultant solution was heated on magnetic stirrer at 80 ^oC with

continuous stirring. During this heating, the pH of the solution was maintained at ~ 7.0 by adding ammonia drop by drop. After small amount of vapors starts coming solution, the temperature of magnetic stirrer was increased to and maintained at 100 ^{o}C. The solution was heated on magnetic stirrer at 100 ^{o}C with continuous stirring for 4 hr. Then solution was found to be converted into viscous gel. Due to constant heating, viscous gel became concentrated and thick and finally at particular moment sudden combustion of thick gel was occurred resulting into fluffy black powder within two min. The fluffy black powder was crushed thoroughly in agate mortar to get fine powder. This fine powder was then heated at 560 ^{o}C for 4 hr in air ambient to obtain the desired composition of ferrite powder. This temperature of annealing of precursor powder was obtained from the TGA/DTA studies. The same procedure was strictly followed to obtain the other desired compositions: $Ni_xCo_{1-x}Dy_yFe_{2-y}O_4$ where, x = 0.1, 0.2, 0.3, 0.4 and y = 0.025 of ferrite powders.

2.3. Characterization of powders

The as-heated resultant ferrite powders were characterized by using different physical techniques. The X-ray diffraction (XRD) patterns of resultant powders recorded by using XRD machine Rigaku, MiniFlex 600 System, Japan, CuK_α radiation, λ = 1.5406 Å were used for the structural analysis. The optical spectra recorded by using the UV-Visible spectrophotometer, UV -2600 Shimadzu, Japan were used to find band gap.

3. Results and discussion

3.1. Thermo-gravimetric (TGA) analysis

The thermo-gravimetric (TGA) analysis was done to understand weight losses at different endothermic and exothermic reactions leading to the stable material. The TGA analysis was also done to obtain the temperature of formation of ferrite powder from the as-combusted precursor. For this purpose, the as-combusted fluffy black powder precursor was subjected for the TGA analysis. For instance, the only one precursor with x = 0.4 and y = 0.025 was taken for TFGA studies. The fig. 1 shows the TGA/DTA plots for the plots for as-combusted fluffy black powder precursor (x = 0.4, y = 0.025).

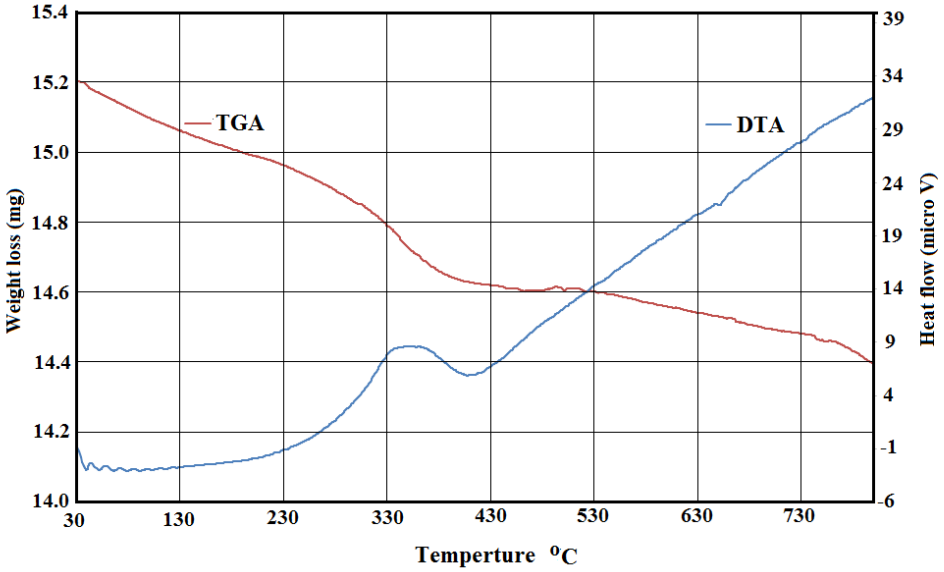

Fig. 1 TGA/DTA plots for as-combusted fluffy black powder precursor (x = 0.4, y = 0.025)

From TGA plot, it is clear that initial weight loss upto 334.48 ^{o}C temperature is 2.63 %. This loss may correspond to removal of the adsorbed water molecules. From 334.48 to 540 ^{o}C, the weight loss = 1.35 % is observed. This weight loss might be due to removal of the trapped gas molecules corresponding to carbon and nitrogen. The weight from 540 to 830 ^{o}C weight loss is also very small equal to 1.36 %. This weight can be assigned to removal residual carbon generated during the auto-combustion of fuel. The temperature above 560 ^{o}C no significant weight loss is observed. Hence 560 ^{0}C is considered as the temperature for the conversion of auto-combusted precursor into the final ferrite powder.

3.2. X-ray diffraction (XRD) analysis

From the TGA analysis the temperature of formation of the ferrite powder from the auto-combusted precursor is around 560 ^{o}C for the composition $Ni_xCo_{1-x}Dy_yFe_{2-y}O_4$ (y = 0.025, and x = 0.4). Hence, for all remaining composition $Ni_xCo_{1-x}Dy_yFe_{2-y}O_4$ (y = 0.025, and x = 0, 0.1, 0.2, and 0.3) the temperature of formation of ferrite powder is considered as 560 ^{o}C. The fig. 2 shows the XRD patterns for as-heated ferrite powders: $Ni_xCo_{1-x}Dy_yFe_{2-y}O_4$ (with y = 0.025, and x = 0, 0.1, 0.2, 0.3, 0.4.

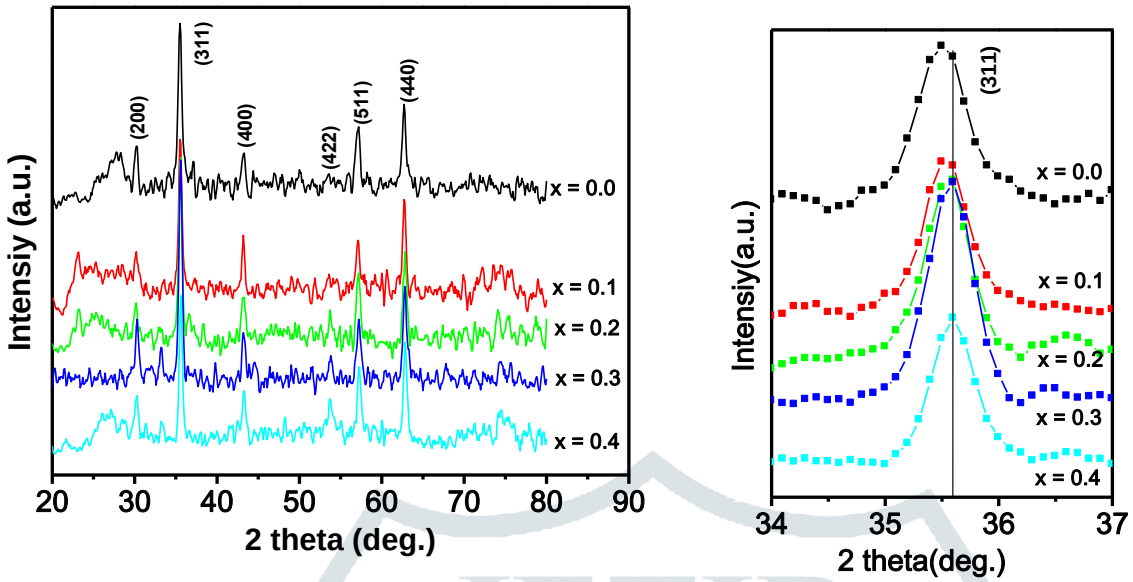

Fig. 2 XRD patterns (left) and slow scans (right) for as-heated ferrite powders: $Ni_xCo_{1-x}Dy_yFe_{2-y}O_4$ (with y = 0.025 and x = 0, 0.1, 0.2, 0.3 and 0.4

All X-ray diffraction patterns for different ferrite powders: $Ni_xCo_{1-x}Dy_yFe_{2-y}O_4$ (with y = 0.025, and x = 0, 0.1, 0.2, 0.3, 0.4 show the same diffraction peaks. All XRD patterns are found to be matching with the each other. In all XRD pattern, peaks corresponding to only spinel phase are observed. This indicates the formation of the phase pure ferrite with spinel symmetry all the resultant powders. The fig. 2 (right) shows the slow scan of the (311) reflections of all XRD patterns of the as-heated ferrite powders: $Ni_xCo_{1-x}Dy_yFe_{2-y}O_4$ (with y = 0.025 and x = 0, 0.1, 0.2, 0.3 and 0.4. The (311) reflection is found to be shifted on the higher angle side. The shift in the diffraction angle is found to be increasing with increasing the concentration of Ni in ferrite phase. It indicates the insertion of Ni at lattice side of Co. All above XRD observation clearly indicates the formation of phase pure $Ni_xCo_{1-x}Dy_yFe_{2-y}O_4$ ferrite powder in present work. The values of crystallite size for resultant ferrite powders are obtained by using Debye-Scherrer relation:

$$D = \frac{0.9\,\lambda}{\beta cos\theta} \qquad \text{- (1)}$$

where, λ = 1.54 A°, β = full width at half maximum and θ = Bragg's diffraction angle. The data for crystallite size for resultant ferrite powders is given in Table 1.

Table 1 Data for average crystallite size

Composition, x	Average crystallite size (nm)
0.0	24.76
0.1	25.87
0.2	38.69
0.3	33.18
0.4	29.26

The average crystallite size is found to be between 24.76 to 38.69 nm. It confirms that ferrites powders are nanocrystalline.

3.3. UV-visible analysis

Fig. 3 shows UV-visible absorbance spectra for as-heated ferrite powders: $Ni_xCo_{1-x}Dy_yFe_{2-y}O_4$ (with y = 0.025 and x = 0, 0.1, 0.2, 0.3 and 0.4. The band gap energy (E_g) is calculated using formula,

$$E_g = \frac{12400}{\lambda} \quad \text{- (2)}$$

Where, λ = wavelength in A^o. Table 2 gives the data for the band gap energy for all ferrite powders. The band gap energy (E_g) is found to be in the range of 1.638 to 1.673 eV indicating thereby semiconductor nature of result ferrite powder.

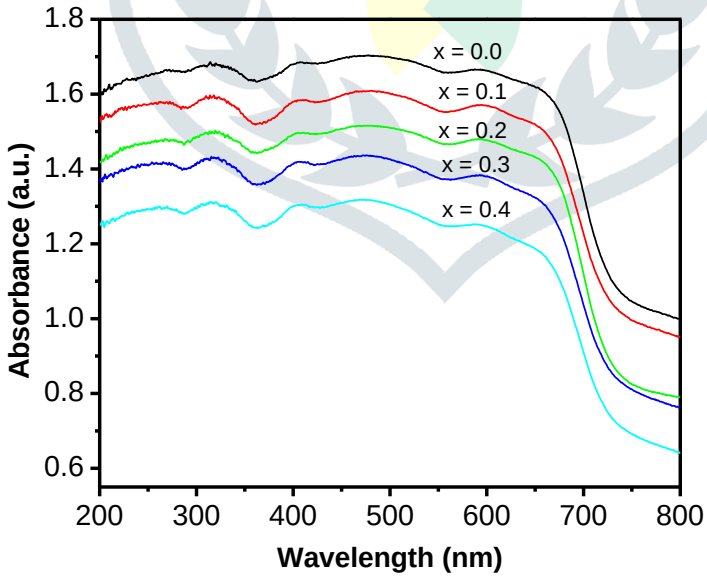

Fig. 3 UV-visible absorbance spectra for as-heated ferrite powders: $Ni_xCo_{1-x}Dy_yFe_{2-y}O_4$ (with y = 0.025 and x = 0, 0.1, 0.2, 0.3 and 0.4

Table 2 Data for band gap energy

Composition x	Wavelength ^{0}A	Band gap energy (ev)
0.0	7461	1.661
0.1	7504	1.652
0.2	7408	1.673
0.3	7486	1.656
0.4	7567	1.638

3.4. FTIR analysis

Fig. 4 shows the FTIR transmission spectra for as-heated ferrite powders: $Ni_xCo_{1-x}Dy_yFe_{2-y}O_4$ (with y = 0.025 and x = 0, 0.1, 0.2, 0.3 and 0.4. From fig. 4, it is clear that, in all FTIR spectra two absorption bands at 565 cm^{-1} and 662 cm^{-1} are seen. These two bands are due to the metal-oxygen vibration in Co_3O_4 spinel oxide. These two bands can be assigned to the stretching vibration of Co-O or Ni-O. Further, the first band at 565 cm^{-1} is associated with OB_3 vibrations in the spinel lattice. In this case the B indicates the Co^{3+} ions in an octahedral hole [28 -29].

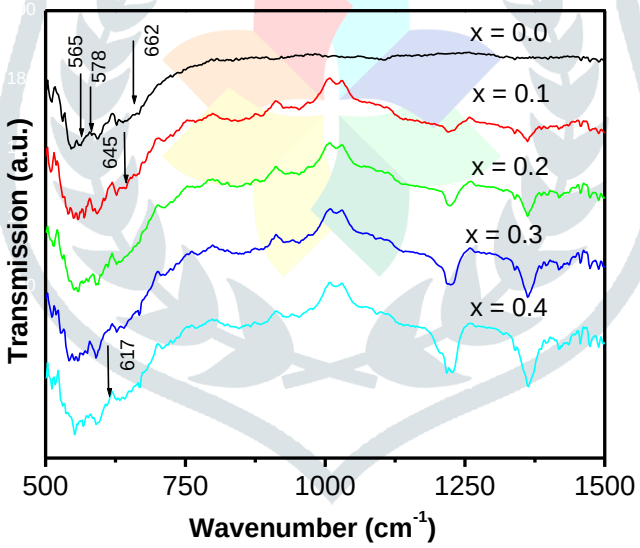

Fig. 4 FTIR transmission spectra for as-heated ferrite powders: $Ni_xCo_{1-x}Dy_yFe_{2-y}O_4$ (with y = 0.025 and x = 0, 0.1, 0.2, 0.3 and 0.4

The second band 662 cm^{-1} is due to the ABO_3 vibration. In this case the A denotes Co^{2+} ions in a tetrahedral hole. All spectra in the fig. 3 also show the three bands at 578, 617 and 645 cm^{-1}. These three bands can attributed to the stretching vibration of the Fe-O bond in the tetrahedral site [28 -29]. Thus FTIR analysis indicates the formation of phase pure ferrite powder in present work.

4. Conclusions

The auto-combustion of co-precipitated gel precursor followed annealing the auto-combusted precursor at elevated temperature is easy and simple processing route for the preparation of ferrite powders. It requires less instrumentation and control over the processing parameter. The method is useful for doping the nickel-cobalt based ferrites. In present work, the cobalt and dysprosium doped nickel ferrite powder processed by using this method is found to be nanocrystalline and phase pure with cubic spinel symmetry.

References

1. Y. H. Kim, S. Hashi, K. Ishiyama, K. I. AraiI, M. Inoue, Remote temperature sensing system using reverberated magnetic flux. IEEE Transactions on Magnetics, 36(5), (2000) 3643 - 3645.
2. V.L.O. Brito, A.C.C. Migliano, L.V. Lemos, F.C.L. Melo, Ceramic processing route and characterization of a Ni-Zn ferrite for application in a pulsed-current monitor, Progress in Electromagnetics Research, 91 (2009) 303 - 318.
3. R. Bergs, R.A. Islam, M. Vickers, H. Stephanou, S. Priya, Magnetic field anomaly detector using magnetoelectric composites. Journal of Applied Physics, 101(2) (2007) 024108.
4. F.F. Stucki, Lockheed Corp., assignee. Ferrimagnetic Pressure Transducer. Great Britain patent GB 1.168.861. 1969 Oct 29.
5. V.L.O. Brito, S.A. Cunha, F.F. Araújo, J.P.B. Machado, M.R. Silva, C. Bormio-Nunes, Processing and characterization of a Ni-Co ferrite for sensor applications, Cerâmica, 61(359) (2015) 341 - 349.
6. M. Sedlar, V. Matejec, I. Paulicka, Optical fibre magnetic field sensors using ceramic magnetostrictive jackets, Sensors & Actuators A: Physical, 84(3) (2000) 297 - 302.
7. P. Samoila, L. Sacarescu, A.I. Borhan, D. Timpu, M. Grigoras, N. Lupu, M. Zaltariov, V. Harabagiu, Magnetic properties of nanosized Gd doped Ni-Mn-Cr ferrites prepared using the sol-gel auto combustion technique, J. Magn. & Magn. Mater., 378 (2015) 92 - 97.
8. K. S. Ramakrishna, Ch. Srinivas, S.S. Meena, B.V. Tirupanyam, Pramod Bhatt, S. M. Yusuf, C.L. Prajapat, D.M. Potukuchi, D.L. Sastry, Investigation of cation distribution and magnetocrystalline anisotropy of $Ni_xCu_{0.1}Zn_{0.9-x}Fe_2O_4$ nanoferrites: role of constant mole percent of Cu^{2+} dopant in place of Zn^{2+}, Ceram. Int., 43 (1) (2017) 7984 - 7991.
9. S.R. Bhongale, H.R. Ingawale, T.J. Shinde, Kunal Pubby, S.B. Narang, P.N. Vasambekar, Nano-crystalline magnesium substituted cadmium ferrites as x band microwave absorbers, J. Magn. & Magn. Mater. 441 (2017) 475 - 481.
10. R. Rajesh Kanna, N. Lenin, K. Sakthipandi, M. Sivabharathy, Impact of lanthanum on structural, optical, dielectric and magnetic properties of $Mn_{1-x}Cu_xFe_{1.85}La_{0.15}O_4$ spinel nanoferrites, Ceram. Int., (2017), https://doi.org/10.1016/j.ceramint.2017.08.160.
11. A. Goldman, Modern Ferrite Technology, New York: Van Nostrand Reinhold; 1990.

12. B.P. Jacob, S. Thankachan, S. Xavier, E.M. Mohammed, Effect of Tb^{3+} substitution on structural, electrical and magnetic properties of sol-gel synthesized nanocrystalline nickel ferrite. J. Alloys & Compd., 578 (2013) 314 - 319.
13. I.H. Gul, A. Masqood, Structural, magnetic and electrical properties of cobalt ferrites prepared by the sol - gel route. J Alloys & Compd., 465 (2008) 227 - 231
14. Z. Zi, Y. Sun, X. Zhu, Song W. Synthesis and magnetic properties of $CoFe_2O_4$ ferrite nanoparticles. J. Magn. & Magn. Mater., 321 (2009) 1251 - 1255.
15. V. Gopalan, P.A. Joy, I. A. Al-Omari, D.S. Kumar, Y. Yoshida, M.R. Anantharaman, On the structural, magnetic and electrical properties of sol - gel derived nanosized cobalt ferrite. J. Alloys & Compd., 485 (2009) 711 - 717.
16. M. George, S.S. Nair, K.A. Malini, P.A. Joy, M.R. Anantharaman, Finite size effects on the electrical properties of sol-gel synthesized $CoFe_2O_4$ powders: Deviation from Maxwell-Wagner theory and evidence of surface polarization effects, J. Magn. & Magn. Mater., 302 (2006) 190 - 195.
17. B.P. Jacob, S. Thankachan, S. Xavier, E.M. Mohammed, Effect of Gd^{3+} doping on the structural and magnetic properties of nanocrystalline Ni-Cd mixed ferrite. Phys. Scr., 84 (2010) 045702 – 6.
18. L. Guo, X. Shen, X. Meng, Y. Feng, Effect of Sm^{3+} ions doping on structure and magnetic properties of nanocrystalline $NiFe_2O_4$ fibers, J. Alloys & Compd., 490 (2010) 301 - 306.
19. A. B. Gadkari, T.J. Shinde, P.N. Vasambekar, Structural synthesis of Y^{3+} doped Mg-Cd ferrites prepared by oxalate co-precipitation method, Mater. Chem. Phys., 114 (2009) 505 - 510.
20. T.J. Shinde, A.B. Gadkari, P.N. Vasambekar, Effect of Nd^{3+} substitution on structural and electrical properties of nanocrystalline zinc ferrite, J. Magn. & Magn. Mater., 322 (2010) 2777 - 2781.
21. K.K. Bamzai, G. Kour, B. Kour, S.D. Kulkarni, Effect of cation distribution on structural and magnetic properties of Dy substituted magnesium ferrite, J. Magn. & Magn. Mater., 327 (2013) 159 - 166.
22. P. Kumar, S.K. Sharma, M. Knobel, M. Singh, Effect of La^{3+} doping on the electric, dielectric and magnetic properties of cobalt ferrite processed by co-precipitation technique, J. Alloys & Compd., 508 (2010) 115 - 118.
23. N. Lenin, A. Karthik, M. Sridharpanday, M. Selvam, S.R. Srither, S. Arunmetha, P. Paramasivam, V. Rajendran, Electrical and magnetic behaviour of iron doped nickel titanate ($Fe^{3+}/NiTiO_3$) magnetic nanoparticles, J. Magn. & Magn. Mater., 397 (2016) 281 -286.
24. Xiangyu Hou, Jing Feng, Xiaodong Xu, Milin Zhang, Synthesis and characterizations of spinel $MnFe_2O_4$ nanorod by seed–hydrothermal route, J. Alloys & Compd., 491 (2010) 258 - 263.
25. Santi Phumying, Sarawuth Labuayai, Ekaphan Swatsitang, Vittaya Amornkitbamrung, Santi Maensiri, Nanocrystalline spinel ferrite (MFe_2O_4, M = Ni Co, Mn, Mg, Zn) powders prepared by a simple aloe vera plant-extracted solution hydrothermal route, Mater. Res. Bull., 48 (2013) 2060 - 2065.

26. Ding Chen, Hong Yan Liu, Lin Li, One-step synthesis of manganese ferrite nanoparticles by ultrasonic wave-assisted ball milling technology, Mater. Chem. Phys., 134 (2012) 921–924.
27. K. Sakthipandi, V. Rajendran, T. Jayakumar, Phase transitions of bulk and nanocrystalline $La_{1-x}Sr_xMnO_3$ (x = 0.35 and 0.37) perovskite manganite materials using in situ ultrasonic studies, Mater. Res. Bull., 48 (2013) 1651- 1659.
28. Ali GAM, O.A. Fouad, S.A. Makhlouf, Structural, optical and electrical properties of sol-gel prepared mesoporous Co_3O_4/SiO_2 nanocomposites, Journal of Alloys and Compounds, 579 (2013) 606 - 611.
29. A. Ammari, B. Bellal, N. Zebbar, B. Benrabah, M. Trari, Thermal-frequency dependence study of the sub-band localized states effect in Sb-doped SnO_2 based sol-gel thin films, Thin Solid Films, 632 (2017) 66 - 72.